



Published in final edited form as:

Biochemistry. 2010 May 11; 49(18): 3815–3823. doi:10.1021/bi902214j.

Probing Soluble Guanylate Cyclase Activation by CO and YC-1 using Resonance Raman Spectroscopy[†]

Mohammed Ibrahim[‡], Emily R. Derbyshire[‡], Michael A. Marletta^{‡,§}, and Thomas G. Spiro^{‡,*}

[‡] Department of Chemistry, University of Washington, Seattle, Washington 98195-1700

[‡] Department of Molecular and Cell Biology, University of California, Berkeley, California 94720-3220

[§] Department of Chemistry, University of California, Berkeley, California 94720-3220

Abstract

Soluble guanylate cyclase (sGC) is weakly activated by CO but is significantly activated by the binding of YC-1 to the sGC-CO complex. In this report resonance Raman (RR) spectroscopy was used to study selected sGC variants. Addition of YC-1 to the sGC-CO complex alters the intensity pattern of RR bands assigned to the vinyl and propionate heme substituents, suggesting changes in the tilting of the pyrrole rings to which they are attached. YC-1 also shifts the RR intensity of the ν_{FeC} and ν_{CO} bands from 473 and 1985 cm^{-1} to 487 and 1969 cm^{-1} , respectively, and induces an additional ν_{FeC} band, at 521 cm^{-1} , assigned to 5-coordinate heme-CO. Site-directed variants in the proximal heme pocket (P118A) or in the distal heme pocket (V5Y and I149Y) reduce the extent of YC-1 activation, along with the 473 cm^{-1} band intensity. These lower activity sGC variants display another ν_{FeC} band at 493 cm^{-1} which is insensitive to YC-1 addition and is attributed to protein that cannot be activated by the allosteric activator. The results are consistent with a model in which YC-1 binding to sGC-CO results in a conformational change that activates the protein. Specifically, YC-1 binding alters the heme geometry via peripheral non-bonded contacts, and also relieves an intrinsic electronic effect that diminishes FeCO backbonding in the native, YC-1 responsive protein. This electronic effect might involve neutralization of the heme propionates via H-bond contacts, or negative polarization by a distal cysteine residue. YC-1 binding also strains the Fe-histidine bond, leading to a population of 5-coordinate sGC-CO in addition to a conformationally distinct population of 6-coordinate sGC-CO. The loss of YC-1 activation in the sGC variants might involve a weakening of the heme-protein contacts which are thought to be critical to a YC-1-induced conformational change.

Soluble guanylate cyclase (sGC) is the key transducer of nitric oxide (NO) signaling in biology (1). In mammals, an array of physiological responses are activated when sGC produces the second messenger cyclic GMP (cGMP) in response to NO binding (1,2).

In addition to NO, sGC binds CO, and there is much interest in the possibility that CO might be a physiologically relevant signaling molecule (3–5). sGC is activated to a small extent by CO, but addition of the synthetic effector molecules YC-1 or BAY 41-2272, to the sGC-CO complex significantly increases sGC activity (6). It has recently been reported that the stoichiometric binding of NO to sGC (1-NO) also generates a low-level activity species (7,8). Like the low-activity sGC-CO complex, the low-activity sGC-NO complex is significantly

[†]This work was supported financially by NIH grants GM033576 (TGS) and GM077365 (MAM)

*To whom correspondence should be addressed. Phone: 206-685-4964, Fax: 206-685-8665, spiro@chem.washington.edu.

activated in the presence of YC-1 (8,9). However, excess NO produces a high activity form of sGC by binding to a non-heme site involving cysteine residues (10), a mechanism not available to CO.

sGC is a heterodimeric protein consisting of an $\alpha 1$ and a $\beta 1$ subunit. The $\beta 1$ subunit consists of Heme Nitric oxide/Oxygen (H-NOX), PAS, CC (coiled-coil) and catalytic domains (Figure 1). The heme cofactor is bound to the $\beta 1$ H-NOX domain, which is a conserved domain of unique structure (11). To date, three wild-type H-NOX domain crystal structures have been reported (12–14). Figure 2 shows a homology model of this domain in sGC based on the crystal structure of the H-NOX domain of a bacterial (*Thermoanaerobacter tengcongensis*, *Tt*) chemoreceptor protein (14). The heme is attached to the protein through the proximal His105 side chain (His102 in *Tt* H-NOX), and a number of peripheral non-bonded contacts. The heme is sandwiched between the proximal and distal halves of the protein, whose relative orientations are somewhat variable in different molecules of the *Tt* H-NOX unit cell. Of particular note is the observation that the residue substitution P115A (P118A in rat sGC $\beta 1$) relaxes the highly distorted heme geometry found in *Tt* H-NOX, and induces a substantial reorientation of the distal (N-terminal) half of the domain (15). This structural change suggests a pathway for signal transmission from the heme to the functional domain (16). Additionally, ligation of *Nostoc* *sp* (*Ns*) H-NOX by NO or CO produces a similar intra-domain reorientation (12).

The binding site for YC-1 is uncertain. Mutational studies had suggested that YC-1 interacts with the catalytic domain (17), but recent biochemical experiments rule this out (18). There is an effector site on the catalytic domain, but it binds nucleotides and not YC-1 (18). Photoaffinity studies with YC-1 analogs have found label on the sGC $\alpha 1$ subunit, specifically at Cys 238 and Cys 243 (19). This finding suggests that YC-1 binds within the linker region between the H-NOX and PAS domains (Figure 1), a proposal which is supported by a study showing elimination of YC-1 activation upon deletion of residues 259–364 on the $\alpha 1$ chain (20). Also, YC-1 binding has been shown to occur in the N-terminal two-thirds of sGC from *Manduca sexta* (21,22). Thus YC-1 likely exerts its effect through an allosteric interaction from a site remote to both the heme and the catalytic center.

In this study we seek to elucidate the YC-1 effect using visible and ultra-violet (UV) resonance Raman spectroscopic methods to probe both the changes in the heme structure and the environment of aromatic residues. YC-1 is found to impose changes in the heme geometry, in the status of the Fe-His bond, in the electronic structure of bound CO, and in the environment around aromatic residues on the $\beta 1$ subunit. The CO effect is used to show that residue substitutions in the heme pocket that diminish YC-1 activation also reduce the spectroscopic signal in proportion. These observations support and extend previous results from the laboratories of Kitagawa (23) and Kincaid (24). Based on our findings, we suggest a model in which YC-1 binding induces a protein conformational change that exerts a torque on the heme, and this YC-1-induced movement is vitiated when the protein-heme contacts are perturbed by activity-impairing residue substitutions.

Methods

Protein expression, purification and activity assay

Rat sGC $\alpha 1\beta 1$ was purified as described previously (25). Rat $\beta 1(1-194)$ and $\beta 1(1-385)$ were purified according to a previously published protocol (11). The $\beta 1(1-194)$ variant P118A and the full-length $\beta 1$ variants V5Y, P118A and I149Y were generated and purified by a method that will be described elsewhere. Additionally, $\beta 1(1-194)$ P118A and $\alpha 1\beta 1$ P118A were purified without heme and reconstituted according to a method that will be described elsewhere.

The activity of the $\alpha 1\beta 1$ variants V5Y, P118A and I149Y was measured in the presence and absence of YC-1 (Cayman Chemical) and CO. CO (g) was added to sGC (233 nM) in 50 mM HEPES, pH 7.4, 50 mM NaCl in an anaerobic cuvette. After complex formation was confirmed by UV-Vis spectroscopy, the protein was added to an assay mixture to initiate the enzyme reaction. The final assay contained 0.2 μ g of enzyme in 50 mM HEPES, pH 7.4, 1 mM DTT, 3 mM $MgCl_2$, 1.5 mM GTP and 150 μ M YC-1 where indicated. All assays were in a final volume of 100 μ L and had a concentration of 2 % DMSO, which was shown not to affect enzyme activity. Reactions were quenched after 3 min by the addition of 400 μ L of 125 mM $Zn(CH_3CO_2)_2$ and 500 μ L of 125 mM Na_2CO_3 . cGMP quantification was carried out using a cGMP enzyme immunoassay kit, Format B (Biomol), per the manufacturer's instructions. Each experiment was repeated 2–4 times to ensure reproducibility.

Resonance Raman (RR) spectroscopy

sGC-CO samples for visible RR experiments were prepared by passing high purity CO gas through ligand-free sGC samples (4–10 μ M in 50 mM HEPES, pH 7.4, 50 mM NaCl, 1 mM DTT) in a septum-sealed NMR tube for ~ 15 min. Formation of the Fe(II)-CO adduct was confirmed by UV-Vis spectroscopy. For UVRR experiments, $\beta 1(1-385)$ -CO samples were prepared in the same manner, except that the protein concentration was higher (50 μ M) and the samples contain 0.2 M sodium perchlorate as an internal standard. YC-1 and BAY 41-2272 (Cayman Chemical)-bound samples were prepared by adding YC-1 and BAY 41-2272 stock in DMSO anaerobically into the CO-bound sample to make final YC-1 and BAY 41-2272 concentrations of 100–150 μ M (~ 2 % [v/v] DMSO).

RR spectra were collected for samples in spinning NMR tubes via backscattering geometry at room temperature. For visible RR experiments, the excitation wavelengths at 430 nm (for ligand-free samples) and 413 nm (for CO-bound samples) were obtained by frequency doubling, using a nonlinear lithium triborate crystal, of a Ti:sapphire laser (Photonics International TU-UV), which was pumped by the second harmonic of a Q-switched Nd:YLF laser (Photonics Industries International, GM-30-527). Laser power at the sample was kept to a minimum (less than 1 mW) by using a cylindrical lens to avoid the photolysis of bound CO. Scattered light was collected and focused onto a single spectrograph (SPEX 1269) equipped with a CCD detector (Roper Scientific) operating at -110 °C. Spectra were calibrated with dimethyl formamide and DMSO. For UVRR experiments, samples were excited at 229 nm from an intracavity doubled-argon ion laser (Innova 300 FReD, Coherent Radiation). Sample degradation was minimized by using low laser power (~0.5 mW at the sample). A single spectrograph (Spex 1269) equipped with a UV enhanced CCD detector (Princeton Instruments) operating at -110 °C was used to collect the scattered light. UVRR spectra were calibrated using acetone. A Grams A/I software (Thermo-Galactic) was used to analyze the spectra.

Results

sGC activity

Included in this study are three variant full-length sGC constructs, with residue substitution in the heme-binding pocket (Figure 2): P118A, V5Y and I149Y. All three proteins with these substitutions have lower enzymatic activity in response to the known activators CO and YC-1 (Table 1). CO addition to the WT enzyme increases the ligand-free basal activity 10-fold, while addition of the effector molecule YC-1 to the Fe(II)-CO complex activates the enzyme an additional 9-fold. The heme pocket mutations produce variable effects on the YC-1-free activities, but all three variants exhibit reduced activation in the presence of YC-1. Specifically, stimulation of the CO adduct by YC-1 is reduced ~3-fold by the P118A and V5Y substitutions, and is completely abolished in the I149Y variant.

Ligand-free RR spectra

RR spectra of the ligand-free sGC variants (Figure 3) show the usual porphyrin vibrational bands (for mode assignments see (26)) expected for 5-c Fe(II) heme, and also the $\nu_{\text{Fe-His}}$ band, which is associated with stretching of the bond between the Fe and the proximal histidine ligand. $\nu_{\text{Fe-His}}$ is found at an unusually low frequency in sGC (204 cm^{-1} (27,28)) indicating a weakened bond relative to other histidine-ligated heme proteins (e.g. 220 cm^{-1} in myoglobin).

The $\nu_{\text{Fe-His}}$ band is unaffected by the V5Y or I149Y substitutions, indicating that the immediate heme environment is similar to that in the wild-type protein. We were unable to record $\nu_{\text{Fe-His}}$ for the P118A variant of full-length sGC, but this substitution produces a slight up-shift (2 cm^{-1}) in $\nu_{\text{Fe-His}}$ in the truncated heme domain $\beta 1(1-194)$ (Figure 3). The truncation itself, however, produces an elevation in the frequency, 204 to 212 cm^{-1} , indicating a somewhat strengthened bond when interactions with other domains are absent.

Most of the porphyrin bands in the Fe(II)-unligated RR spectra are not affected by the residue substitutions, except for small changes in relative intensities. The 760 cm^{-1} ν_{15} band is shifted down 13 cm^{-1} in the $\beta 1(1-194)$ truncation when compared to the full-length sGC constructs. Additionally, the 419 cm^{-1} vinyl side chain bending mode observed in sGC V5Y is shifted down 3 cm^{-1} in sGC I149Y, WT $\beta 1(1-94)$ and $\beta 1(1-94)$ P118A. These shifts indicate subtle changes in porphyrin conformation.

Notably, P118A in $\beta 1(1-94)$ has no effect on the porphyrin bands except for the disappearance of a weak 321 cm^{-1} band, identified as the γ_{16} out-of-plane mode. The homologous mutation in the *Tt* H-NOX domain (P115A) relaxes the heme distortion found in the WT structure (15). In the RR spectrum of *Tt* H-NOX, this relaxation led to a lower intensity for a number of out-of-plane RR bands in the O_2 complex (29). The spectrum of the ligand-free variant *Tt* H-NOX showed no detectable RR changes compared to the WT spectrum except for a slight up-shift in the $\nu_{\text{Fe-His}}$ band, similar to that seen here for $\beta 1(1-94)$ P118A.

RR spectra of CO adducts and YC-1 effects

The CO adducts of WT sGC and the sGC variants were examined by RR spectroscopy. The sGC porphyrin bands undergo characteristic shifts upon CO binding (Figures 4 and 5), and the RR spectra of the CO adducts also show ν_{FeC} and ν_{CO} bands, at ~ 490 and $\sim 1970\text{ cm}^{-1}$, associated with stretching of the Fe-C and C-O bonds of the bound CO. WT sGC has two bands for each of these modes (Figure 4), a dominant pair at 473 and 1985 cm^{-1} , and a weaker pair at 487 and 1969 cm^{-1} (the WT ν_{CO} bands are not shown in Figure 4, since they have been previously reported (23, 24)). In agreement with earlier studies, addition of YC-1 switches these pairs, so that the 487 and 1969 cm^{-1} bands become dominant. In addition, a new ν_{FeC} band appears at 521 cm^{-1} , characteristic of 5-c Fe(II)heme-CO. Thus, we observed that YC-1 binding to the CO adduct leads to the breaking of the Fe-His bond in an unknown fraction of the protein population. These effects are accentuated when the more potent effector BAY 41-2272 is added to the CO adduct. Specifically, the 521 cm^{-1} band is augmented and the 473 and 1985 cm^{-1} bands are diminished further. The ν_{CO} bands are generally weak in RR spectra making them difficult to deconvolute. However, Martin *et al.* have shown via infrared spectroscopy (24) that the 1969 cm^{-1} band produced by BAY 41-2272 addition to the sGC-CO complex is actually a composite of bands at 1972 and 1964 cm^{-1} . They were able to assign the 1964 cm^{-1} band to the 5-c heme-CO species, on the basis of its temperature dependence.

In addition, YC-1 decreases the intensity of the 424 cm^{-1} RR band but increases the intensity at 398 , 370 , and 308 cm^{-1} (Figure 4). BAY 41-2272 again shows the same changes but with greater magnitude. The 424 and 398 cm^{-1} bands are assigned to bending vibrations of the 2- and 4-vinyl heme substituents, respectively, the 370 cm^{-1} band is assigned to a propionate

bend, and the 308 cm^{-1} band is likely an out-of-plane porphyrin deformation, γ_7 (26). A similar pattern of vinyl and propionate intensity alteration has been seen upon YC-1 addition to the NO adduct of sGC, and was attributed to changes in the heme out-of-plane distortion, involving tilting of the pyrrole rings to which the vinyl and propionate groups are attached (30), producing net planarization of the heme.

The effect of YC-1 on the RR spectra of the sGC variants was also examined. The P118A, V5Y and I149Y variants have ν_{FeC} bands at 493 cm^{-1} , but P118A and V5Y have a shoulder at 473 cm^{-1} , which decreases upon YC-1 addition (Figure 5). This shoulder is undetectable for the I149Y variant, with or without YC-1. In the ν_{CO} region, a weak 1988 cm^{-1} band in the P118A spectrum disappears on YC-1 addition and the dominant 1969 cm^{-1} band is augmented. A similar effect is seen in the V5Y spectrum, although the frequencies are slightly lower, 1984 and 1960 cm^{-1} , suggesting an influence of the V5Y substitution on the environment of the bound CO. ν_{CO} was undetectable for the I149Y variant due to low signal/noise. Additionally, a split ν_4 in the I149Y spectrum indicates photolysis of the Fe-CO bond occurs both in the presence and absence of YC-1.

Significantly, the presence of the 473 cm^{-1} shoulder, and its diminution by YC-1 correlates with the degree of activation by YC-1; YC-1-induced activity is greatly diminished in the P118A and V5Y variants and abolished in the I149Y variant (Table 1). To investigate this spectra/function correlation further, the ν_{FeC} band envelope was deconvoluted and the relative area of the 473 cm^{-1} component was plotted against the relative degree of YC-1 activation of the Fe(II)-CO complex (Table 1). The straight line defined by WT sGC (100%) and the I149Y variant (0%), passes close to the points for P118A (35%) and V5Y (38%) (Figure 6). Thus, the 473 cm^{-1} ν_{FeC} component represents that fraction of sGC molecules that is activatable by YC-1.

UVRR spectra of $\beta 1(1-85)$

The heme-binding domain of sGC has a single tryptophan residue, Trp22 (Figure 1 and 2), which appears to be in a region that is responsive to the heme conformation based on a mutational study with *Tr* H-NOX (15) (Figure 2). Consequently, we examined the effect of CO and YC-1 binding on the 229 nm-excited UVRR spectrum, in which tryptophan and tyrosine vibrational bands are selectively enhanced (31,32). The $\beta 1(1-85)$ construct was chosen for this experiment because it has only one tryptophan residue (full-length sGC has five, three in the $\alpha 1$ subunit and two in the $\beta 1$ subunit), and because it is known (33,34) to retain the property of having 473 and 1985 cm^{-1} ν_{FeC} and ν_{CO} bands which are diminished by YC-1.

Figure 7 shows that YC-1 increases the intensity of both tyrosine (Y8a/b, Y9a, Y7a) and tryptophan (W3, W7, W16, W17) bands, indicating environmental changes of the aromatic rings. The intensity change suggests that Trp22 becomes less exposed to solvent (31) upon YC-1 addition. The tyrosine signals are harder to interpret since $\beta 1(1-385)$ has 14 tyrosine residues.

The UVRR spectrum of ligand-free $\beta 1(1-85)$ (not shown) was indistinguishable from that of the CO adduct, indicating that any CO-induced protein conformation change was undetectable by the aromatic residue probes.

Discussion

Three spectroscopic states of sGC-CO are linked to activity

The RR spectral responses to specific sGC variants, and to the binding of the effector molecules YC-1 or BAY 41-2272, allow us to identify three states of sGC-CO (Table 2).

- State I is associated with the majority population in WT sGC-O, which has ν_{FeC} and ν_{CO} at 473 and 1985 cm^{-1} . This population significantly decreases when YC-1 or BAY 41-2272 is added to WT sGC-CO. The sGC variants P118A and V5Y have minority populations of state I, which also disappear upon effector addition, whereas no population of state I is observed in sGC I149Y.
- State II is associated with the majority population when effectors are bound to sGC-CO. A larger state II fraction is induced by BAY 41-2272 than by YC-1. A small state II fraction is already present in WT sGC-CO. State II has a mixture of 6- and 5-coordinate heme-CO adducts, with ν_{FeC} and ν_{CO} at 487 and 1972 cm^{-1} , and at 521 and 1964 cm^{-1} , respectively. Although the 6-coordinate fraction appears to be dominant, it is not possible to quantify the ratio of 5- and 6-coordinate fractions, because their molar RR intensities are unknown.
- State III is brought about by the mutations P118A, V5Y and I149Y; it has ν_{FeC} and ν_{CO} at 493 and 1968 cm^{-1} , and is unaffected by addition of effectors. The state III positions are close to those of the 6-coordinate fraction of state II, and the bands cannot readily be deconvoluted. It is possible that WT sGC-CO has a small population of state III as well as a population of state II.

These spectroscopically defined states can be linked to a functional model through the activity data in Table 1. The shift from state I to state II is associated with the shift from low to high activity when YC-1 is added to sGC-CO. Moreover, the extent of state I diminution upon YC-1 addition correlates quantitatively with the extent of YC-1 activation (Figure 6). Thus state II represents high-activity enzyme, while state I represents protein that is capable of high activity upon effector binding. It is likely that the modest activity of effector-free sGC-CO reflects the minority state II population that it contains. Meanwhile state III represents protein that is incapable of being activated by YC-1. Only state III is detectable for the I149Y variant, which is unresponsive to YC-1. State III is dominant for the P118A and V5Y variants, which exhibit a minor state I fraction and a decrease in YC-1-induced activation when compared to WT sGC (Figure 6).

Our model suggests that sGC is poised for activation in state I, and becomes active in state II. The binding of CO to sGC may produce a small population of state II while effector binding to sGC-CO produces a significant population of state II. However, the required transition of state I to II can be lost by residue substitutions that alter the structure sufficiently to leave variable fractions of the protein in a form, characterized as state III, which is incapable of being activated.

Structure of the spectroscopic states

The ν_{FeC} and ν_{CO} frequencies of state I, 473 and 1985 cm^{-1} , are unusually low and high, respectively, compared to other heme protein CO adducts. Because of FeCO backbonding, ν_{FeC} and ν_{CO} frequencies are anti-correlated, and the $\nu_{\text{FeC}}/\nu_{\text{CO}}$ plot gives information about the influence of protein interactions that affect backbonding (35). Figure 8 shows the correlation seen for heme proteins and model complexes having an imidazole ligand *trans* to the CO (6-c) and also for 5-c CO-heme. Shown for illustration are $\nu_{\text{FeC}}/\nu_{\text{CO}}$ points for myoglobin (Mb) and for its H64V variant in which the distal His residue, whose NH group provides positive polarity and increases backbonding (35), is replaced by a hydrophobic residue. The result of this replacement is to shift the point down the line, the direction of less backbonding. The $\nu_{\text{FeC}}/\nu_{\text{CO}}$ points for state III and the 6-coordinate fraction of state II of sGC-CO are close to the H64V variant of Mb, indicating a hydrophobic environment for the bound CO and a normal imidazole *trans* ligand.

The $\nu_{\text{FeC}}/\nu_{\text{CO}}$ point for state I also lies on the correlation, indicating an intact Fe-His bond, but at a much lower position, reflective of anomalously weak backbonding. Similarly, weakened backbonding has been detected for the H64V/V68T variant of Mb (Figure 8), in which the introduced threonine side chain is oriented (via H-bonding to a backbone carbonyl) so that its O atom lone pair points at the bound CO (36). This orientation weakens backbonding through negative polarity (35,36). A homology model based on the *Tt* H-NOX structure (Figure 2) suggests that the distal heme pocket in sGC is lined with hydrophobic residues, except for Cys78. The homologous residue in *Tt* H-NOX, Phe78, is close enough to the heme that an introduced OH substituent (F78Y) can donate an H-bond to a heme ligand, as evidenced by restoration of O₂ affinity in a *Tt* H-NOX variant that can not bind O₂ (Y140L) (37,38). It is, therefore, conceivable that Cys78 could provide negative polarity to the bound CO in sGC, if the SH group were properly oriented, as the Thr68 OH group is oriented in the H64V/V68T variant of Mb. A structural change upon YC-1 binding could readily abolish the hypothesized Cys78 interaction and shift the $\nu_{\text{FeC}}/\nu_{\text{CO}}$ point up the backbonding line to a position characteristic of a hydrophobic pocket, as is seen in state II. Since state III occupies a similar position one could infer that a different structural change that produces protein incapable of activation also abolishes the Cys78 interaction with the bound CO. In future studies, the proposed role of Cys78 will be investigated by replacing it with apolar residues.

We have recently suggested an alternative explanation for weakened backbonding in sGC-CO, namely strong H-bonding to the heme propionate substituents (39). DFT calculations indicate that neutralization of the propionate negative charges would weaken FeCO backbonding through an inductive effect, and would shift the $\nu_{\text{FeC}}/\nu_{\text{CO}}$ frequencies by the same magnitude as observed in the state I/II transition (39). The *Tt* H-NOX crystal structure (14) shows the propionate groups to be buried and tightly bound to positively charged and H-bond donating residues. Both propionates interact with Arg135, and one of them accepts H-bonds from Ser133 and Tyr131. These three residues form the YxSxR motif found in all H-NOX domains, including that of the sGC β 1 subunit. The shift from state I to II RR signals could then be explained if YC-1 induces a protein structural change that breaks or weakens these propionate contacts. Again, the near coincidence of state II and III signals would imply a different, activity-impairing structural change that also weakens the propionate contacts in state III.

A third alternative is that the anomalously low backbonding in state I results from out-of-plane distortion of the heme ring, a prominent feature of the *Tt* H-NOX structure (14). In this scenario, the YC-1-induced protein structural change would allow the porphyrin to relax, restoring the backbonding. Again, the activity-impairing structural change in state III would likewise relax the porphyrin distortion. However, relaxation of the porphyrin distortion via P115A substitution in *Tt* H-NOX was found to have no effect on the ν_{FeC} position in the CO adduct (29). This negative result is consistent with earlier DFT calculations (39) which predicted insignificant effects of porphyrin distortion on the FeCO vibrational frequencies. The porphyrin distortion is no doubt linked to the propionate contacts, and if the latter are weakened the porphyrin may well relax. However it is the propionate contacts that would be the primary determinants of the FeCO frequencies in such a coupled structural change.

A YC-1-induced effect on the heme is also evidenced by the altered intensities of RR bands associated with the peripheral vinyl and propionate substituents in state II (Figure 4). However, these changes are not those expected from relaxation of the porphyrin distortions based on studies with *Tt* H-NOX. Tran et al. (29) found that RR changes associated with the heme-flattening in the P115A variant involved intensity losses for a number of bands in the 500–1000 cm⁻¹ region, which is associated with pyrrole distortion and methine C-H out-of-plane modes. However, the vinyl and propionate mode intensity changes and the γ_7 intensification observed here were not seen with that mutation. Thus, the YC-1 induced changes are not simply due to porphyrin relaxation, but must be associated with an enforced geometry change, which

produces net planarization. The transition to this altered form results in strengthened FeCO backbonding, due either to a loss of a possible Cys78 lone pair interaction with the CO or with weakening of the propionate H-bonds from the YxSxR residues. We note independent evidence from CO and NO rebinding kinetics that YC-1 alters the structure of the heme pocket (25, 40).

The sGC variants examined in this study, which result in a significant population of state III and reduced YC-1 activation, involve the modification of residues in the heme pocket (Figure 2). One of these residues, P118, likely influences the heme via non-bonding interactions and thus may be involved in porphyrin distortion (15). The V5Y and I149Y substitutions introduce bulky and polar residues, which may perturb the structure-maintaining heme-protein contacts. Therefore all three variants may shift the protein to state III by a similar mechanism; however it remains to be determined if heme distortion is requisite for sGC activation.

Activation mechanism and the role of Fe-His dissociation

A critical feature of sGC activation by NO is the dissociation of the Fe-histidine bond (41), which is induced by the strong *trans* effect of NO when bound to Fe(II). This dissociation triggers a conformation change in the protein leading to activation. The weakness of the Fe-His bond in ligand-free sGC, reflected in the low $\nu_{\text{Fe-His}}$ frequency (Figure 3), suggests that the protein is primed for this dissociation event. In addition, studies of metalloporphyrin binding to apo-sGC have shown significant activity levels when the metal fails to bind histidine (Ni(II), Cu(II)) (42) or when the porphyrin lacks a metal, but no activation occurs when the metal does bind histidine (Fe(II), Co(II), Mn(II)) (43). Similarly, the physiological effect of NO-bound H-NOX protein from *Shewanella oneidensis*, namely inhibition of a histidine kinase autophosphorylation, is weak for the CO adduct compared to the NO complex (44). However, the CO complex of the proximal histidine variant where heme binding is rescued with imidazole has activity approaching that of the NO complex (16). The NMR structure of this variant reveals a relaxed heme and a reorientation of the two halves of the H-NOX domain (16). Thus the status of the heme-proximal-histidine linkage plays an integral part in structural changes associated with activity in H-NOX domains.

However, it is now known that the stoichiometric binding of NO to sGC activates the enzyme only modestly, in fact to about the same extent as CO binding (8). The binding of this single molecule of NO results in the dissociation of the Fe-His bond, but clearly the sGC-NO species is not fully activated. The observation of a low-activity 5-coordinate sGC-NO complex suggests that Fe-His dissociation is not sufficient to fully activate sGC, which requires the binding of effectors, or of additional NO (10).

On the other hand, the appearance of a 5-c CO-heme signal upon YC-1 addition to sGC-CO, and its increase in the presence of BAY 41-2272, does correlate high-level activation with Fe-His dissociation from some of the heme. We infer that formation of state II produces stress on the Fe-His bond, and shifts the equilibrium between 6- and 5-c CO-heme toward the 5-c form.

Other structural consequences of ligation must also be important. The Fe(II) metal lies out of the heme plane in the resting 5-c state and it is drawn into the plane by exogenous ligand binding. The heme is held firmly by many non-bonded protein contacts, including the propionate YxSxR interactions mentioned above.

We envision that a torque is applied to the protein as the NO or CO draws the Fe(II) toward the distal side (Figure 9). This movement possibly involves a pivot and bend of the heme, as described by Ma et al. for a cyanobacterial H-NOX domain, *Ns* H-NOX (12). Through the non-bonded contacts, this torque could be coupled to a large-scale protein displacement, likely similar to the N-terminal displacement seen in the *Tt* H-NOX (15) and *Ns* H-NOX (12)

structures. It is this displacement that the Trp22 UVRR intensities may be sensing (Figure 7). Additionally, this protein displacement could trigger an activating conformational change in the catalytic domain, via inter-domain contacts. Through an allosteric interaction the binding of effector molecules would then increase the torque and therefore the level of activation (State II). However, alterations in the heme-protein non-bonded contacts, through perturbing residue replacements, would have the effect of slipping the clutch and reducing the attainable torque (State III).

In this scenario, the status of the Fe-His bond is an indicator of the torque level. For NO, the low-level torque produced by ligation is sufficient to break the Fe-His bond, because of the NO *trans* effect, which weakens the Fe-His bond. However, for CO, whose electronic effect is to strengthen the *trans* bond (45), the high-level YC-1-induced torque is required to produce partial Fe-His dissociation.

Acknowledgments

We thank Rosalie Tran and Richard Mathies for preliminary RR characterization of the Fe(II)-unligated β 1(1-194) P118A construct.

Abbreviations

sGC	soluble guanylate cyclase
CO	carbon monoxide
NO	nitric oxide
YC-1	3-(5'-hydroxy-methyl-3'-furyl)-1-benzylindazole
RR	resonance Raman
cGMP	cyclic guanosine 3',5'-monophosphate
BAY 41-2272	5-cyclopropyl-2-{1-(2-fluorobenzyl)-1H-pyrazolo[3,4-b]pyridin-3-yl}pyrimidin-4-ylamine
H-NOX	heme nitric oxide/oxygen binding
<i>Tt</i>	<i>Thermoanaerobacter tengcongensis</i>
<i>Ns</i>	<i>Nostoc sp</i>
HEPES	4-(2-hydroxyethyl)-1-piperazineethanesulfonic acid
DTT	dithiothreitol
GTP	guanosine 5'-triphosphate
DMSO	dimethyl sulfoxide
Ti	sapphire, titanium sapphire
Nd	YLF, neodymium doped yttrium lithium fluoride
CCD	charge coupled device
WT	wild type
6-c	six-coordinate
5-c	five-coordinate
UVRR	ultra-violet resonance Raman
DFT	density functional theory

NMR nuclear magnetic resonance

References

1. Derbyshire, ER.; Marletta, MA. Biochemistry of soluble guanylate cyclase. In: Schmidt, HHHW.; Hofmann, F.; Stasch, J-P., editors. Handbook of Experimental Pharmacology. Springer-Verlag; Berlin Heidelberg: 2009. p. 17-31.
2. Kots, AY.; Martin, E.; Sharina, IG.; Murad, F. A short history of cGMP, guanylyl cyclases, and cGMP-dependent protein kinases. In: Schmidt, HHHW.; Hofmann, F.; Stasch, J-P., editors. Handbook of Experimental Pharmacology. Springer-Verlag; Berlin Heidelberg: 2009. p. 1-14.
3. Ingi T, Cheng J, Ronnett GV. Carbon monoxide: an endogenous modulator of the nitric oxide-cyclic GMP signaling system. *Neuron* 1996;16:835–842. [PubMed: 8608001]
4. Ndisang JF, Tabien HE, Wang R. Carbon monoxide and hypertension. *Journal of Hypertension* 2004;22:1057–1074. [PubMed: 15167436]
5. Boehning D, Snyder SH. Novel neural modulators. *Annual Review of Neuroscience* 2003;26:105–131.
6. Stasch, J-P.; Hobbs, AJ. NO-independent, heme-dependent soluble guanylate cyclase stimulators. In: Schmidt, HHHW.; Hofmann, F.; Stasch, J-P., editors. Handbook of Experimental Pharmacology. Springer-Verlag; Berlin Heidelberg: 2009. p. 277-308.
7. Russwurm M, Koesling D. NO activation of guanylyl cyclase. *EMBO Journal* 2004;23:4443–4450. [PubMed: 15510222]
8. Cary SPL, Winger JA, Marletta MA. Tonic and acute nitric oxide signaling through soluble guanylate cyclase is mediated by nonheme nitric oxide, ATP, and GTP. *Proceedings of the National Academy of Sciences of the United States of America* 2005;102:13064–13069. [PubMed: 16131543]
9. Schmidt K, Schrammel A, Koesling D, Mayer B. Molecular mechanisms involved in the synergistic activation of soluble guanylyl cyclase by YC-1 and nitric oxide in endothelial cells. *Molecular Pharmacology* 2001;59:220–224. [PubMed: 11160856]
10. Fernhoff NB, Derbyshire ER, Marletta MA. A nitric oxide/cysteine interaction mediates the activation of soluble guanylate cyclase. *Proceedings of the National Academy of Sciences of the United States of America* 2009;106:21602–21607. [PubMed: 20007374]
11. Karow DS, Pan D, Davis JH, Behrends S, Mathies RA, Marletta MA. Characterization of functional heme domains from soluble guanylate cyclase. *Biochemistry* 2005;44:16266–16274. [PubMed: 16331987]
12. Ma X, Sayed N, Beuve A, van den Akker F. NO and CO differentially activate soluble guanylyl cyclase via a heme pivot-bend mechanism. *EMBO Journal* 2007;26:578–588. [PubMed: 17215864]
13. Nioche P, Berka V, Vipond J, Minton N, Tsai AL, Raman CS. Femtomolar sensitivity of a NO sensor from *Clostridium botulinum*. *Science* 2004;306:1550–1553. [PubMed: 15472039]
14. Pellicena P, Karow DS, Boon EM, Marletta MA, Kuriyan J. Crystal structure of an oxygen-binding heme domain related to soluble guanylate cyclases. *Proceedings of the National Academy of Sciences of the United States of America* 2004;101:12854–12859. [PubMed: 15326296]
15. Olea J, Charles Boon EM, Pellicena P, Kuriyan J, Marletta MA. Probing the function of heme distortion in the H-NOX family. *ACS Chemical Biology* 2008;3:703–710. [PubMed: 19032091]
16. Erbil WK, Price MS, Wemmer DE, Marletta MA. A structural basis for H-NOX signaling in *Shewanella oneidensis* by trapping a histidine kinase inhibitory conformation. *Proceedings of the National Academy of Sciences of the United States of America* 2009;106:19753–19760. [PubMed: 19918063]
17. Russwurm M, Mergia E, Mullershausen F, Koesling D. Inhibition of deactivation of NO-sensitive guanylyl cyclase accounts for the sensitizing effect of YC-1. *Journal of Biological Chemistry* 2002;277:24883–24888. [PubMed: 11978784]
18. Derbyshire ER, Fernhoff NB, Deng S, Marletta MA. Nucleotide regulation of soluble guanylate cyclase substrate specificity. *Biochemistry* 2009;48:7519–7524. [PubMed: 19527054]

19. Stasch JP, Becker EM, Alonso-Alija C, Apeler H, Dembowski K, Feurer A, Gerzer R, Minuth T, Perzborn E, Pleiss U, Schroder H, Schroeder W, Stahl E, Steinke W, Straub A, Schramm M. NO-independent regulatory site on soluble guanylate cyclase. *Nature* 2001;410:212–215. [PubMed: 11242081]
20. Koglin M, Behrends S. A functional domain of the alpha1 subunit of soluble guanylyl cyclase is necessary for activation of the enzyme by nitric oxide and YC-1 but is not involved in heme binding. *Journal of Biological Chemistry* 2003;278:12590–12597. [PubMed: 12560334]
21. Hu X, Murata LB, Weichsel A, Brailey JL, Roberts SA, Nighorn A, Montfort WR. Allosteric in recombinant soluble guanylyl cyclase from *Manduca sexta*. *Journal of Biological Chemistry* 2008;283:20968–20977. [PubMed: 18515359]
22. Hu X, Feng C, Hazzard JT, Tollin G, Montfort WR. Binding of YC-1 or BAY 41–2272 to soluble guanylyl cyclase induces a geminate phase in CO photolysis. *Journal of the American Chemical Society* 2008;130:15748–15749. [PubMed: 18980304]
23. Li Z, Pal B, Takenaka S, Tsuyama S, Kitagawa T. Resonance Raman evidence for the presence of two heme pocket conformations with varied activities in CO-bound bovine soluble guanylate cyclase and their conversion. *Biochemistry* 2005;44:939–946. [PubMed: 15654750]
24. Martin E, Czarnecki K, Jayaraman V, Murad F, Kincaid JR. Resonance Raman and infrared spectroscopic studies of high-output forms of human soluble guanylyl cyclase. *Journal of the American Chemical Society* 2005;127:4625–4631. [PubMed: 15796527]
25. Winger JA, Derbyshire ER, Marletta MA. Dissociation of nitric oxide from soluble guanylate cyclase and heme-nitric oxide/oxygen binding domain constructs. *Journal of Biological Chemistry* 2007;282:897–907. [PubMed: 17098738]
26. Hu S, Smith KM, Spiro TG. Assignment of protoheme resonance Raman spectrum by heme labeling in myoglobin. *Journal of the American Chemical Society* 1996;118:12638–12646.
27. Deinum G, Stone JR, Babcock GT, Marletta MA. Binding of nitric oxide and carbon monoxide to soluble guanylate cyclase as observed with resonance Raman spectroscopy. *Biochemistry* 1996;35:1540–1547. [PubMed: 8634285]
28. Tomita T, Ogura T, Tsuyama S, Imai Y, Kitagawa T. Effects of GTP on bound nitric oxide of soluble guanylate cyclase probed by resonance Raman spectroscopy. *Biochemistry* 1997;36:10155–10160. [PubMed: 9254612]
29. Tran R, Boon EM, Marletta MA, Mathies RA. Resonance Raman spectra of an O₂-binding H-NOX domain reveal heme relaxation upon mutation. *Biochemistry* 2009;48:8568–8577. [PubMed: 19653642]
30. Ibrahim M, Derbyshire ER, Soldatova AV, Marletta MA, Spiro TG. Soluble guanylate cyclase is activated differently by excess NO and by YC-1: Resonance Raman spectroscopic evidence. accepted.
31. Chi Z, Asher SA. UV Raman determination of the environment and solvent exposure of Tyr and Trp residues. *Journal of Physical Chemistry B* 1998;102:9595–9602.
32. Balakrishnan G, Weeks CL, Ibrahim M, Soldatova AV, Spiro TG. Protein dynamics from time resolved UV Raman spectroscopy. *Current Opinion in Structural Biology* 2008;18:623–629. [PubMed: 18606227]
33. Schelvis JPM, Zhao Y, Marletta MA, Babcock GT. Resonance Raman characterization of the heme domain of soluble guanylate cyclase. *Biochemistry* 1998;37:16289–16297. [PubMed: 9819221]
34. Denniger JW, Schelvis JPM, Brandish PE, Zhao Y, Babcock GT, Marletta MA. Interaction of soluble guanylate cyclase with YC-1: Kinetic and resonance Raman studies. *Biochemistry* 2000;39:4191–4198. [PubMed: 10747811]
35. Spiro, TG.; Ibrahim, M.; Wasbotten, IH. CO, NO and O₂ as vibrational probes of heme protein active sites. In: Ghosh, A., editor. *The smallest biomolecules: Diatomics and their interactions with heme proteins*. Elsevier; Amsterdam: 2008. p. 96-123.
36. Phillips GN Jr, Theodoro ML, Li TS, Olson JA. Bound CO is a molecular probe of electrostatic potential in the distal pocket of myoglobin. *Journal of Physical Chemistry B* 1999;103:8817–8829.
37. Boon EM, Huang SH, Marletta MA. A molecular basis for NO selectivity in soluble guanylate cyclase. *Nature Chemical Biology* 2005;1:53–59.

38. Boon EM, Marletta MA. Sensitive and selective detection of nitric oxide using an H-NOX domain. *Journal of the American Chemical Society* 2006;128:10022–10023. [PubMed: 16881625]
39. Xu C, Ibrahim M, Spiro TG. DFT analysis of axial and equatorial effects on heme–CO vibrational modes: Applications to CooA and H-NOX heme sensor proteins. *Biochemistry* 2008;47:2379–2387. [PubMed: 18217776]
40. Kharitonov VG, Sharma VS, Magde D, Koesling D. Kinetics and equilibria of soluble guanylate cyclase ligation by CO: Effect of YC-1. *Biochemistry* 1999;38:10699–10706. [PubMed: 10451364]
41. Stone JR, Marletta MA. Spectral and kinetic studies on the activation of soluble guanylate cyclase by nitric oxide. *Biochemistry* 1996;35:1093–1099. [PubMed: 8573563]
42. Carr HS, Tran D, Reynolds MF, Burstyn JN, Spiro TG. Activation of soluble guanylyl cyclase by four-coordinate metalloporphyrins: Evidence for a role for porphyrin conformation. *Biochemistry* 2002;41:10149–10157. [PubMed: 12146980]
43. Dierks EA, Hu S, Yu A, Spiro TG, Burstyn JN. Demonstration of the role of scission of the proximal histidine-iron bond in the activation of soluble guanylyl cyclase through metalloporphyrin substitution studies. *Journal of the American Chemical Society* 1997;119:7316–7323.
44. Price MS, Chao LY, Marletta MA. *Shewanella oneidensis* MR-1 H-NOX regulation of a histidine kinase by nitric oxide. *Biochemistry* 2007;46:13677–13683. [PubMed: 17988156]
45. Ibrahim M, Xu C-L, Spiro TG. Differential sensing of protein Influences by NO and CO vibrations in heme adducts. *Journal of the American Chemical Society* 2006;128:16834–16845. [PubMed: 17177434]

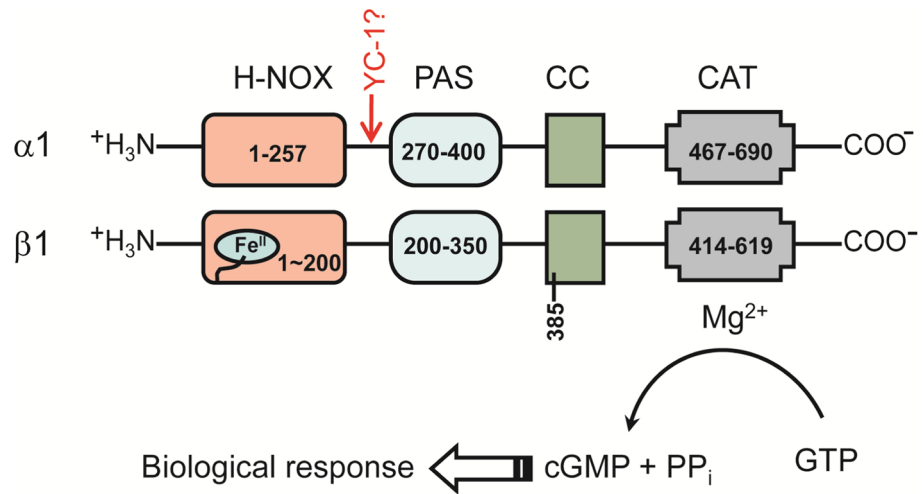


Figure 1. Domain structure of sGC (adapted from (1)). The H-NOX, PAS, CC (coiled coil) and catalytic (CAT) domains are shown.

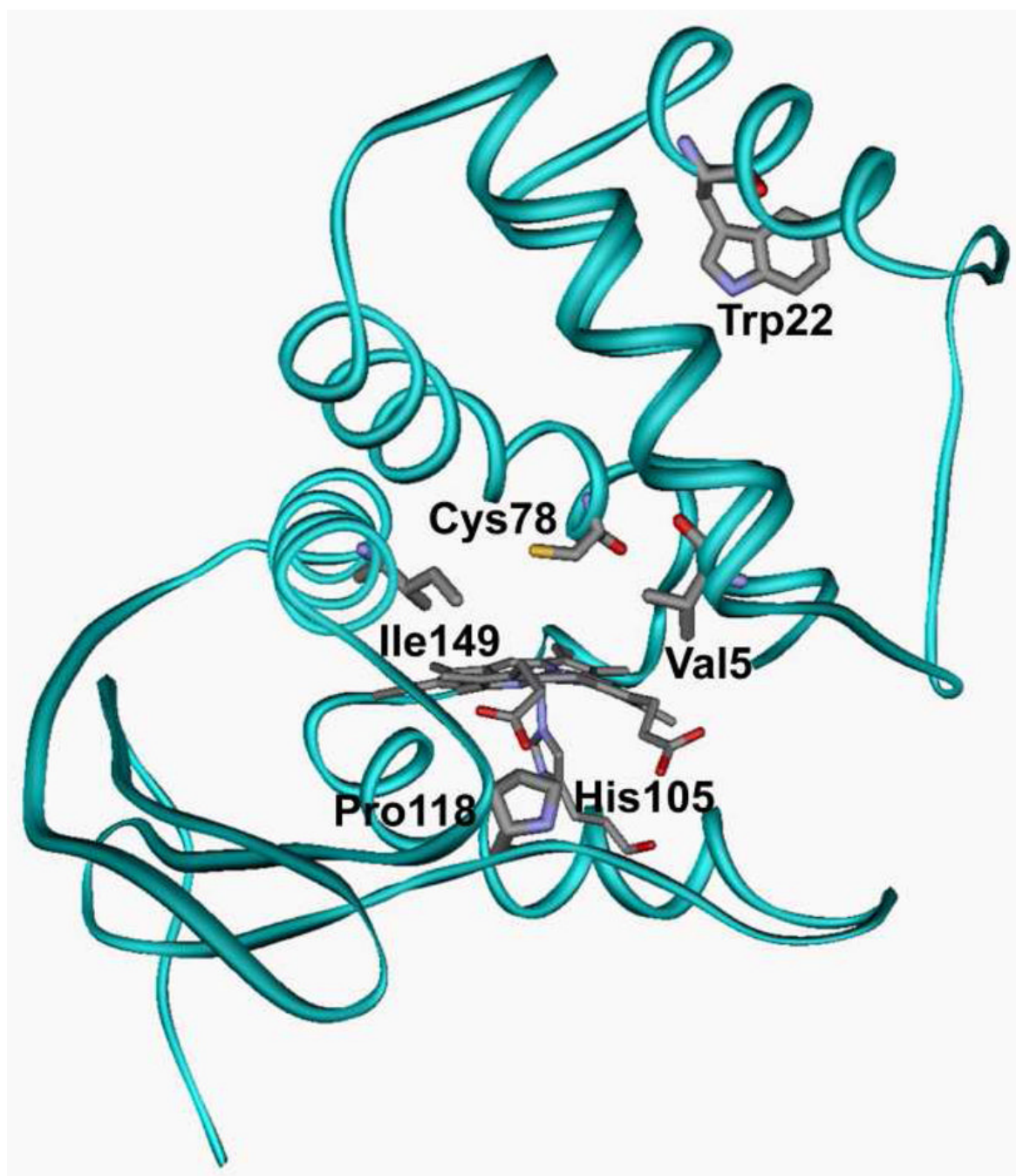


Figure 2. Homology model of the rat sGC β 1 H-NOX domain (based on *Tt* H-NOX structure, pdB: 1U55).

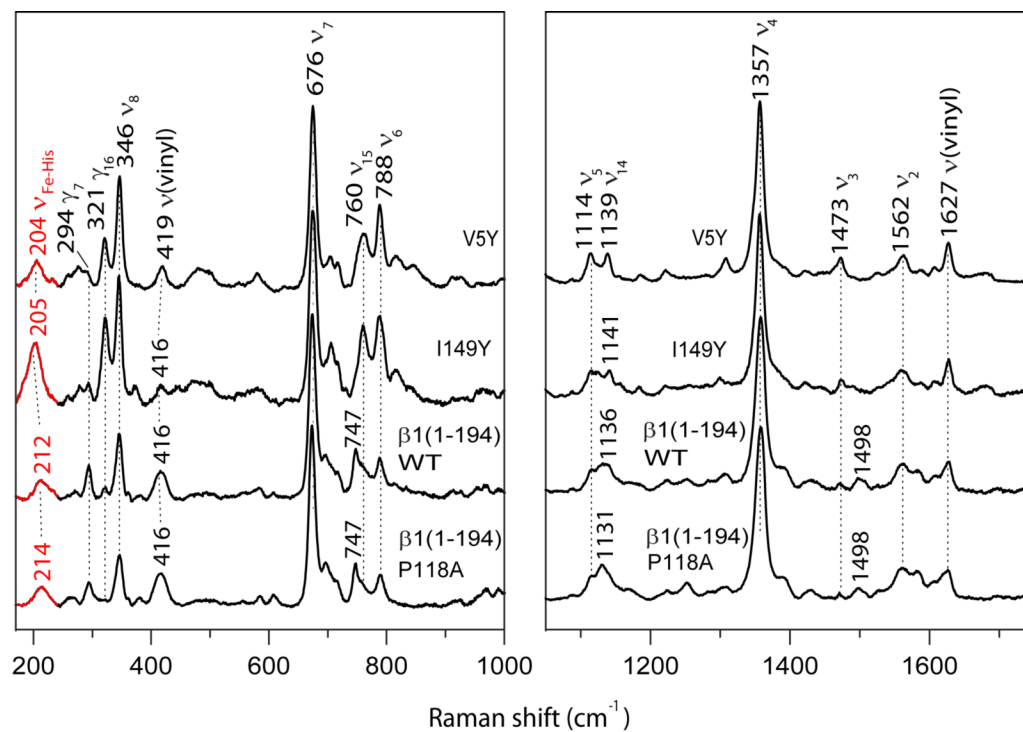


Figure 3. 430 nm-excited RR spectra of the ligand-free forms of V5Y and I149Y full-length Fe(II) sGC (top two spectra) and of the WT and P118A β1(1-194) truncate (bottom two spectra). Band assignments (26) and frequencies are indicated. The Fe-His stretching bands are highlighted.

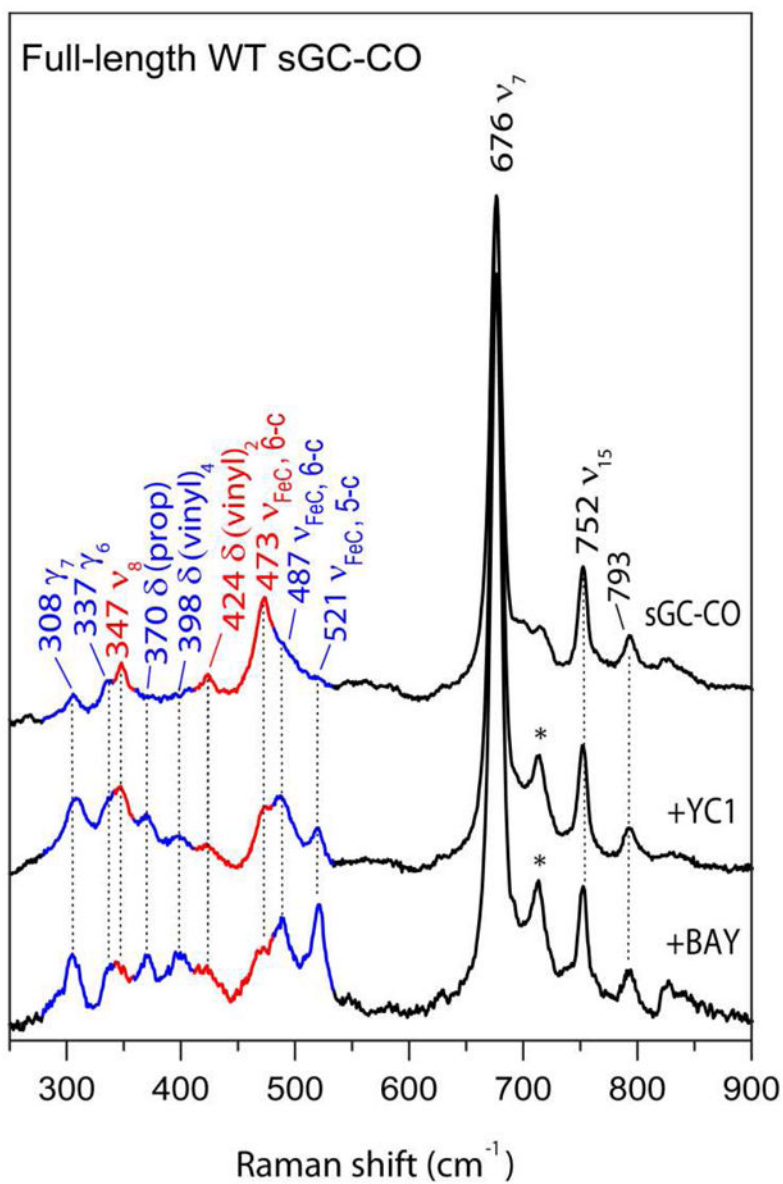


Figure 4. WT sGC-CO RR spectral changes produced by YC-1 and BAY 41-2272 at 413 nm-excitation. Asterisks denote DMSO bands. Red and blue colors indicate bands whose relative intensity decrease or increase, respectively, upon effector binding.

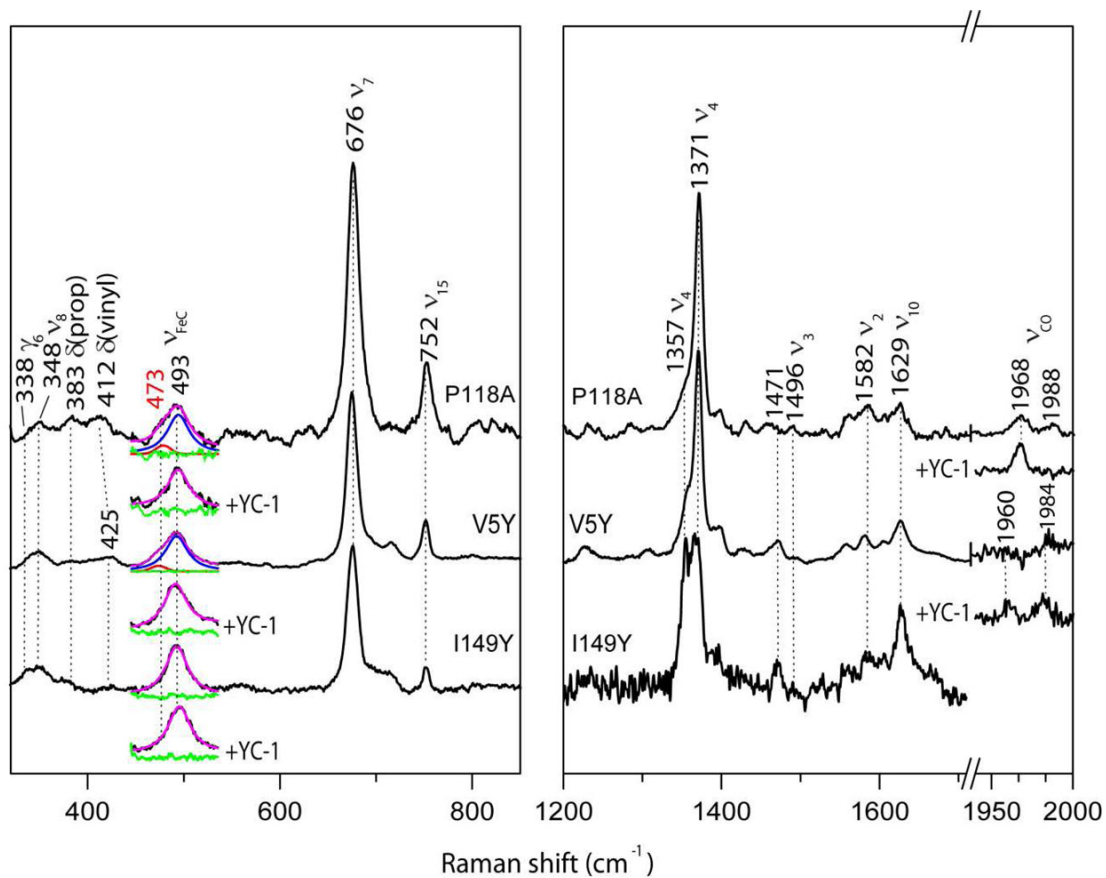


Figure 5. 413 nm-excited RR spectra of CO adducts of P118A, V5Y and I149Y full-length sGC variants, and the effect of YC-1 addition on the v_{FeC} and v_{CO} bands (insets). Insets: traces in black and magenta are original and fitted spectra, respectively. Traces in red and blue are individual peaks that contribute to the fitted spectrum. Trace in green is the residual spectrum (original-fit).

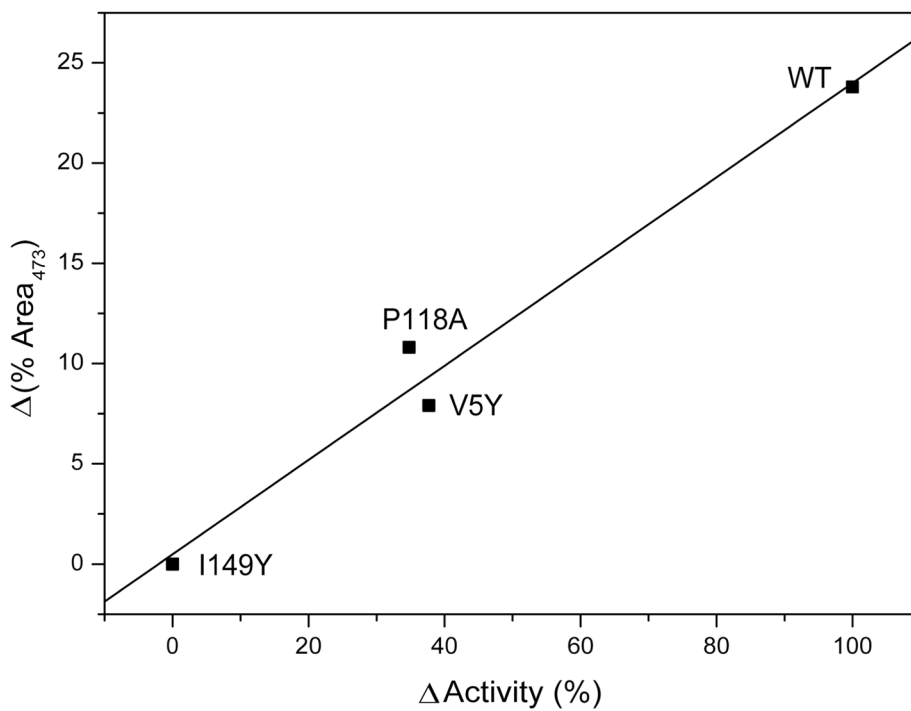


Figure 6. Correlation of $\sim 473\text{ cm}^{-1}$ vFeC fraction with relative YC-1 activation of the indicated sGC-CO adducts.

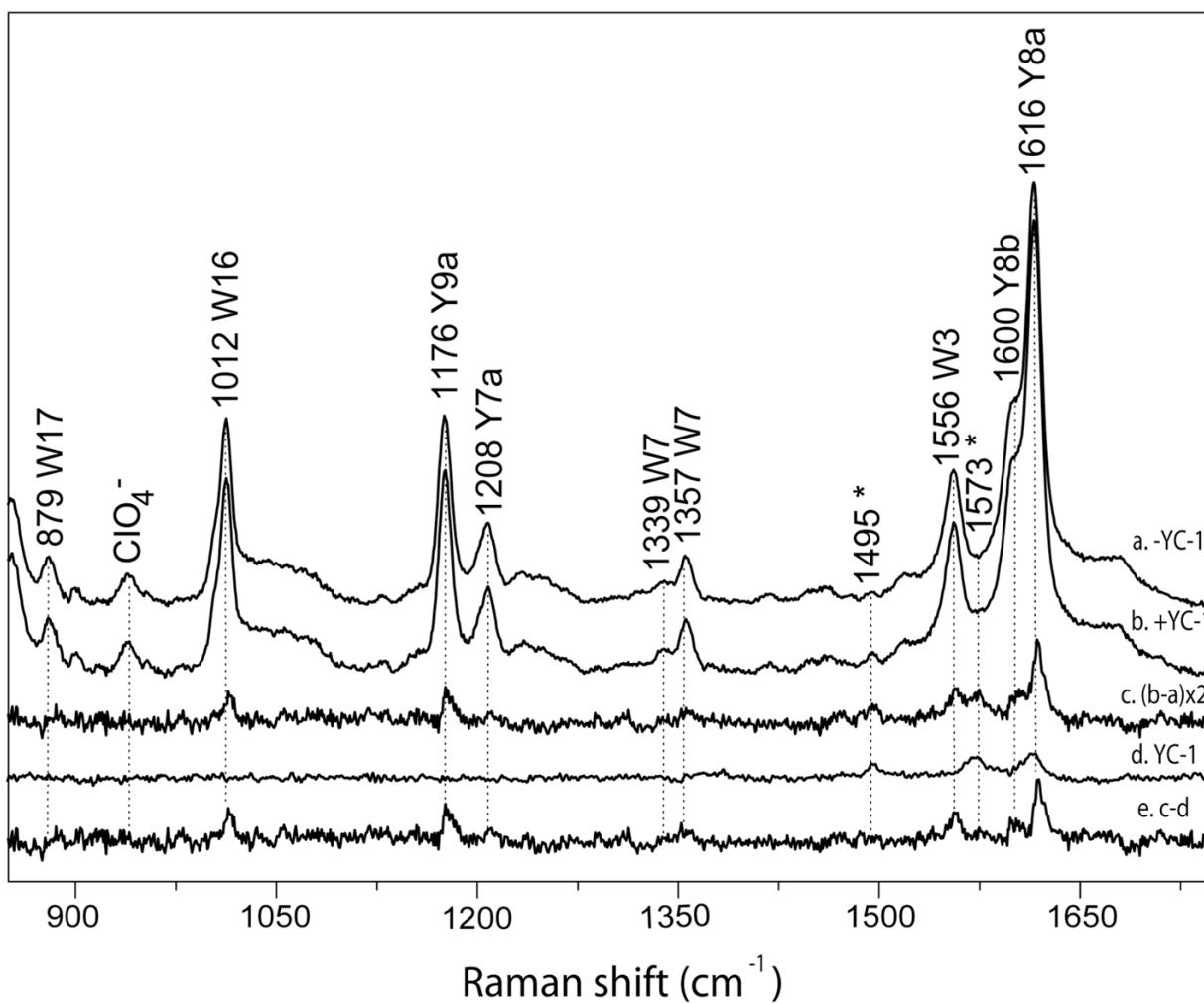


Figure 7. 229 nm-excited UVRR spectra of the CO adduct of sGC β 1(1-385), before and after YC-1 addition (a and b, respectively). The YC-1 UVRR spectrum (d) was recorded separately and subtracted from the difference spectrum (c), to yield the intrinsic changes (e) of the protein. In obtaining the difference spectrum (e), YC-1 spectrum (d) was normalized to spectrum (c) by equalizing the height of the 1573 cm⁻¹ YC-1 band.

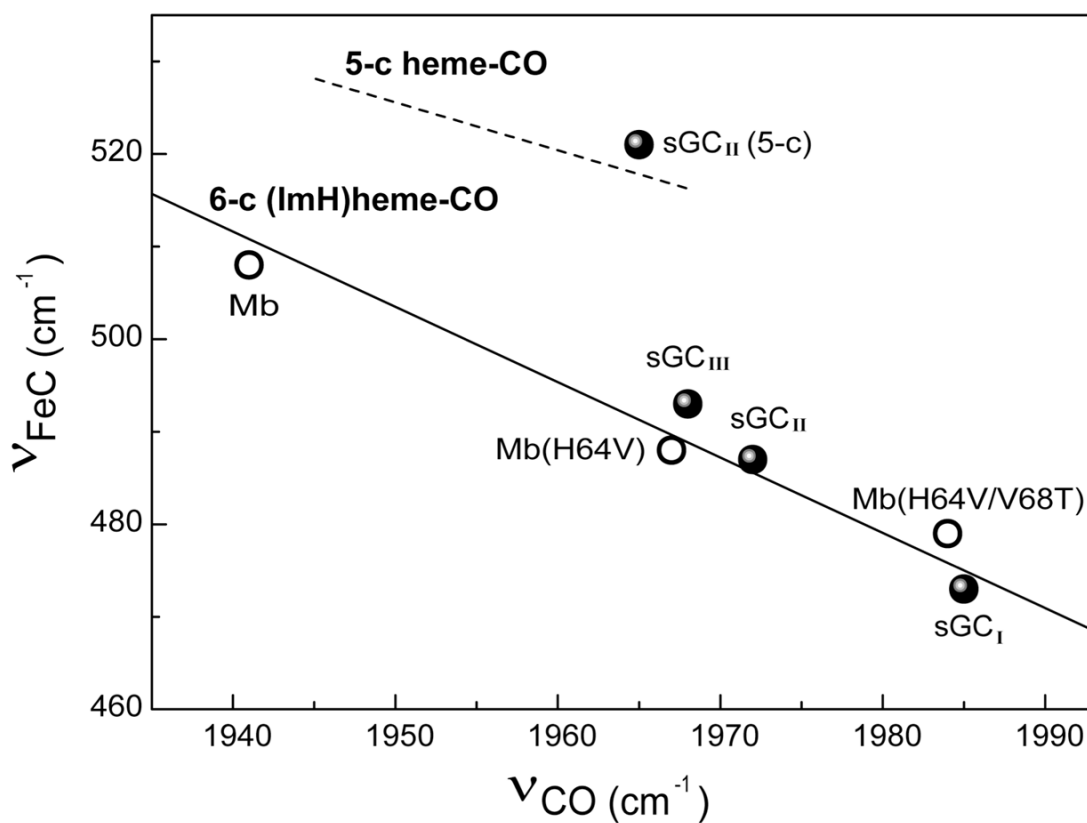


Figure 8. Backbonding plot for heme-CO adducts. The dashed and solid lines are published correlations for 5-c heme-CO and for 6-c (ImH)heme-CO adducts, respectively. The open circles are data (35) for myoglobin (Mb) and its H64V (the positively polar distal His is replaced by the non-polar Val, diminishing the FeCO backbonding) and H64V/V68T (a lone-pair donor interaction from the introduced Thr reduces backbonding further) variants. The filled circles are data for sGC in states I, II and III. sGC_I shows anomalously weak backbonding, while sGC_{II} and sGC_{III} are at positions expected for a hydrophobic heme pocket. sGC_{II} also has a 5-c heme-CO fraction.

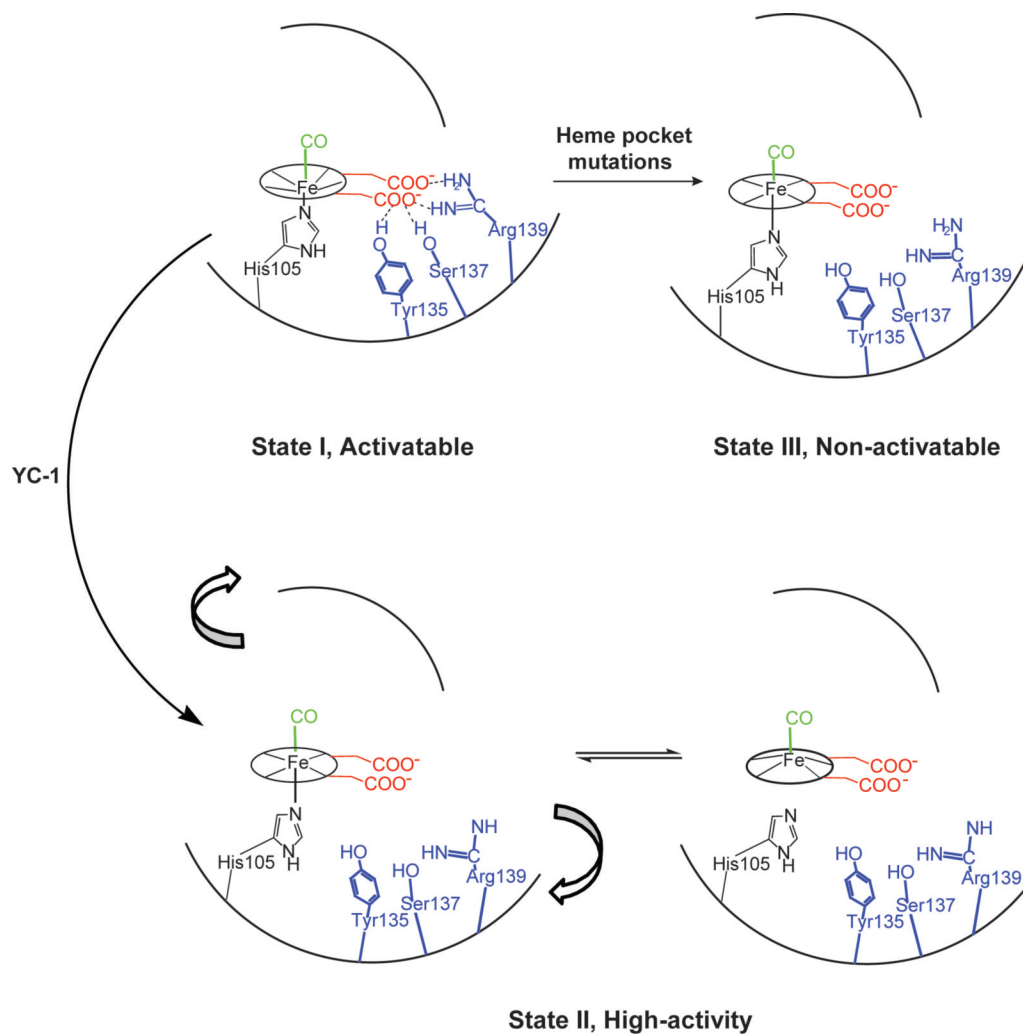


Figure 9.

Structural model for the activation-linked transitions of sGC-CO. In state I, the binding of CO pulls the Fe toward the heme plane, and induces porphyrin distortion via protein contacts. These contacts include strong H-bonds from the YxSxR residues, and possibly from a lone-pair interaction of a distal residue, Cys78 (not shown), with the bound CO; either of these contacts might account for the anomalously weak back-bonding in state I (see text). In state III, the protein contacts are loosened, e.g. by residue substitutions in the heme pocket, relaxing the heme, and rendering the enzyme incapable of activation. In state II, a hypothesized torque, promoted by effector binding, induces heme planarization, abolishes the YxSxR and/or the Cys78 interactions, and breaks the Fe-His105 bond in a fraction of the molecules. The torque is suggested to accompany an activity-inducing rotation of the N-terminal half of the H-NOX domain (15). A small population of state II pre-exists in the effector-free CO adduct, likely accounting for its modest activity.

Table 1

The effect of YC-1 on the sGC-CO activity levels and the ~473 cm⁻¹ RR band intensity

sGC variants	Specific activity (nmol/min/mg)		Δ Activity ^a (nmol/min/mg)	Δ Activity (%) ^b	%Δ ₄₇₃		Δ(%Δ) ₄₇₃ ^c
	-YC-1	+YC-1			-YC-1	+YC-1	
WT CO-free	13 ± 2.4	86 ± 65	73	7.2	-	-	-
WT	134 ± 20	1143 ± 98	1009	100	36.5	12.7	23.8
P118A	18 ± 5.1	369 ± 91	351	34.8	10.8	0	10.8
V5Y	43 ± 0.3	423 ± 90	380	37.7	7.9	0	7.9
I149Y	250 ± 82	185 ± 61	0	0	0	0	0

^a Δ Activity = (Specific activity)+YC-1 - (Specific activity)-YC-1

^b Δ Activity (%) = (Δ Activity)/variant/(Δ Activity)WT × 100

^c Δ (%Δ)₄₇₃ = [(A₄₇₃/A_{total})-YC-1 - (A₄₇₃/A_{total})+YC-1] × 100

Table 2RR band positions (cm^{-1}) for spectroscopically defined states of sGC-CO

State	ν_{FeC}	ν_{CO}
I	473	1985
II	487, 521 ^a	1972, 1964 ^{a,b}
III	493	1968

^a5-coordinate heme-CO fraction^bIR spectral assignment (24)